# Vibrational Study of Some Low-Dimensional Niobium–Phosphorus–Sulfide Compounds, $P_2NbS_8$, $PNb_2S_{10}$, and $P_2Nb_4S_{21}$

M. QUEIGNEC, M. EVAIN, AND R. BREC

*Laboratoire de Chimie des Solides, L.A. 279 CNRS, 2 rue de la Houssinière, 44072 Nantes, France*

AND C. SOURISSEAU

*Laboratoire de Spectrométrie Infrarouge, L.A. 124 CNRS, Université de Bordeaux I, 33405 Talence, France*

Infrared and Raman spectra (800–100 cm$^{-1}$) of polycrystalline samples of 2D $P_2NbS_8$, 3D $P_2NbS_8$, 2D $PNb_2S_{10}$, and 2D $P_2Nb_4S_{21}$ at 300 K were investigated and compared with those of $NbS_2Cl_2$ and of various phosphorus–sulfide anion containing salts. A complete assignment of the spectra is proposed and it emphasizes structural relationships within this niobium–phosphorus–sulfide family, and several modes are assigned to $(Nb_2(S_2)_2)$ cluster motions. The UV-visible absorption spectra (250–1000 nm) of the four compounds exhibit optical band gaps at ~300 nm, which confirms their broadband semiconductor property and an electric dipole allowed charge transfer (Nb → S) transition at about 370–400 nm. This transition can account for selective intensity enhancements of some Raman bands due to $(Nb_2(S_2)_2)$ cluster vibrations under preresonance conditions ($\lambda_0$ = 514.5–488.0 nm). Finally, this vibrational study permits identification of several characteristic modes, such as $\nu$Nb–S, $\nu$Nb–Nb, $\nu PS_2$, or $\nu PS_3$ and stretching of $S_2^{2-}$ or $S_3^{2-}$ groups, which could be perturbed upon further intercalation reactions within the Van der Waals gaps of the two-dimensional host lattices and thus could be used as "electronic probes." © 1986 Academic Press, Inc.

## Introduction

Two-dimensional (2D) and three-dimensional (3D) $P_2NbS_8$, 2D $PNb_2S_{10}$, and 2D $P_2Nb_4S_{21}$ are highly colored diamagnetic insulators. They represent four structural types of a homogeneous family whose structures have been recently determined (*1–4*) and are based on different arrangements of biprismatic bicapped $(Nb_2S_{12})$ units and tetrahedral $(PS_4)$ groups.

The present study has been undertaken as a part of a more general vibrational study of 2D compounds able to intercalate molecules or ions (*5, 6*). In fact, intercalation experiments within the van der Waals gaps (~3.3 Å) of these layered systems are now in progress to search for new materials of interest in electrochemistry as positive electrodes in secondary generators.

The main purpose of this study is thus to identify and compare typical vibrational modes in these host lattices in order to get a better insight into their short-range order and the interatomic interactions around the possible redox centers. This study should

permit some predictions concerning struc-
tural and electronic perturbations induced
by future intercalation reactions.

## Experimental

The four P–Nb–S compounds under
study were prepared as described recently
(1–4) and the $NbS_2Cl_2$ compound was ob-
tained according to literature procedures
(7–9).

UV-Visible absorption spectra (250–1000
nm) were recorded at 300 K using a Cary 17
spectrometer in the transmission mode, and
infrared spectra (1000–180 $cm^{-1}$) were ob-
tained at 300 and 80 K with a Perkin–Elmer
180 instrument, with the powdered samples
being dispersed in Nujol.

Raman spectra (1000–50 $cm^{-1}$) were re-
corded on a triple monochromator Coderg
T800 instrument, using different emission
lines of a Spectra-Physics Model 171 $Ar^+$
laser. Detection through a RCA C31034
photomultiplier was made by standard pho-
ton counting techniques. Low laser power
was always used ($P_0 \le 100$–200 mW), and
spectra of the compounds dispersed in KCl
(KBr or $KClO_4$) were obtained by use of a
sample holder rotating at ca. 1600 rev $min^{-1}$
in order to avoid any local heating effects.
Under these conditions, all the compounds
were quite stable, although $Nb_2S_2Cl_2$ has
been previously reported to decompose
rapidly in the laser beam (10).

## Structures and Selection Rules

The structure of the four P–Nb–S mate-
rials is built of tetrahedral ($PS_4$) groups and
of distorted trigonal bicapped ($NbS_8$)
prisms sharing a rectangular face to consti-
tute ($Nb_2S_{12}$) units (Fig. 1). In each ($Nb_2S_{12}$)
biprism, there is a $Nb^{4+}$–$Nb^{4+}$ single bond
lying perpendicular to the common face
formed by two $S_2^{2-}$ pairs. When looking at
interatomic distances (1–4), the strongest
short-range interactions are localized
within cage-shaped ($Nb_2(S_2)_2$) units. As
similar cages are already known to exist in
niobium–chalcogenide halides $NbS_2X_2$ (7–
12), we have made use of the $NbS_2Cl_2$
model system (see below).

### $NbS_2Cl_2$

This compound crystallizes in the mono-
clinic system, space group $C2/m$ ($C_{2h}^3$), with
two molecular entities per primitive unit
cell (7, 9). The Bravais cell contains only
one ($Nb_2(S_2)_2$) cage of approximately $D_{2h}$
symmetry which consists of a pair of $Nb^{4+}$
ions lying perpendicular to the plane of two
$S_2^{2-}$ groups. The cages are linked together
by the Cl atoms to form sheets parallel to
the (a,b) plane and each metal ion is coordi-
nated to four Cl atoms and to two $S_2^{2-}$ pairs.
However, Nb · · ·Cl interactions are mark-
edly weaker than the Nb · · · S ones, so
that the 12 vibrational modes of an "iso-
lated" ($Nb_2(S_2)_2$) cluster can be classified as
follows:

$$\Gamma^{D_{2h}} \text{ cluster} = 3A_g + B_{2g} + B_{1g} + B_{3g} + A_u + B_{2u} + 2B_{1u} + 2B_{3u}$$

$$\Gamma^{C_{2h}} \text{ crystal} = \underset{\text{(Raman)}}{4A_g} + \underset{\text{(Raman)}}{2B_g} + \underset{\text{(IR)}}{2A_u} + \underset{\text{(IR)}}{4B_u}$$

One expects six Raman and six infrared ac-
tive vibrations with mutual exclusion and
all these modes, labeled from $M_1$ to $M_{12}$ are
sketched in Fig. 2. It is noteworthy that we
have not used the same numbering of vibra-
tions as in Ref. (11) and we propose a
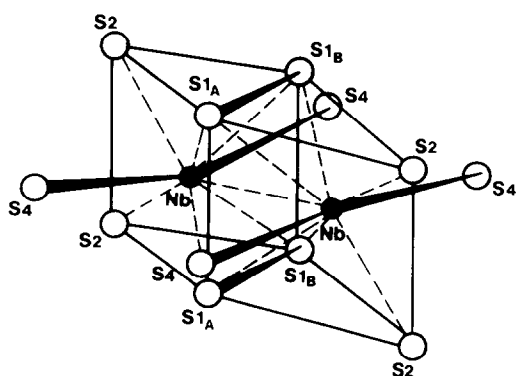slightly different representation of the nor-
mal modes.

FIG. 1. Perspective view of a $(Nb_2S_{12})$ biprismatic bicapped unit showing $(S1_A–S1_B)^{2-}$ pairs (*1*).

## 2D and 3D $P_2NbS_8$

2D $P_2NbS_8$ crystallizes in the orthorhombic $Cmca$ ($D_{2h}^{18}$) space group with four entities per primitive unit cell. The $(Nb_2S_{12})$ units are linked to each other through $(P_2S_6)$ groups made from two edge-sharing $(PS_4)$ tetrahedra giving rise to

$$\left[ PS_2 \diagdown^{S}\diagup_{S} PS_2 \right]^{2-}$$
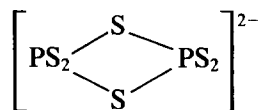
anions (Fig. 3).

3D $P_2NbS_8$ derivative crystallizes in the tetragonal $P\bar{4}m2$ ($D_{2d}^8$) space group with four formula in the Bravais cell. Now, the $(Nb_2S_{12})$ biprisms are bonded to each other
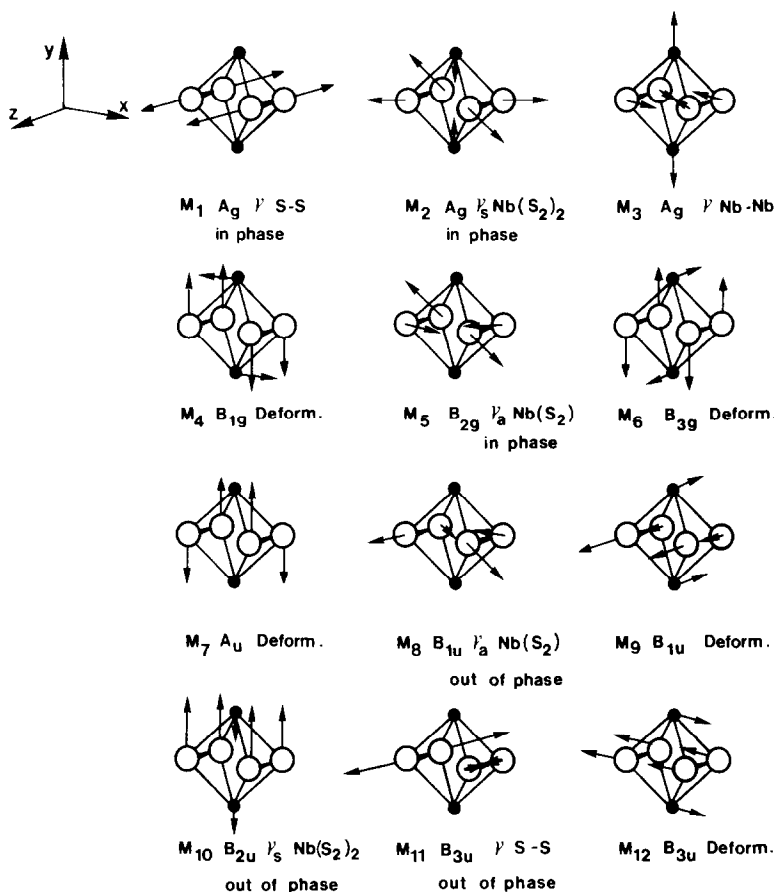


FIG. 2. Schematic representation of the 12 internal vibrations in a $(Nb_2(S_2)_2)$ cage unit.
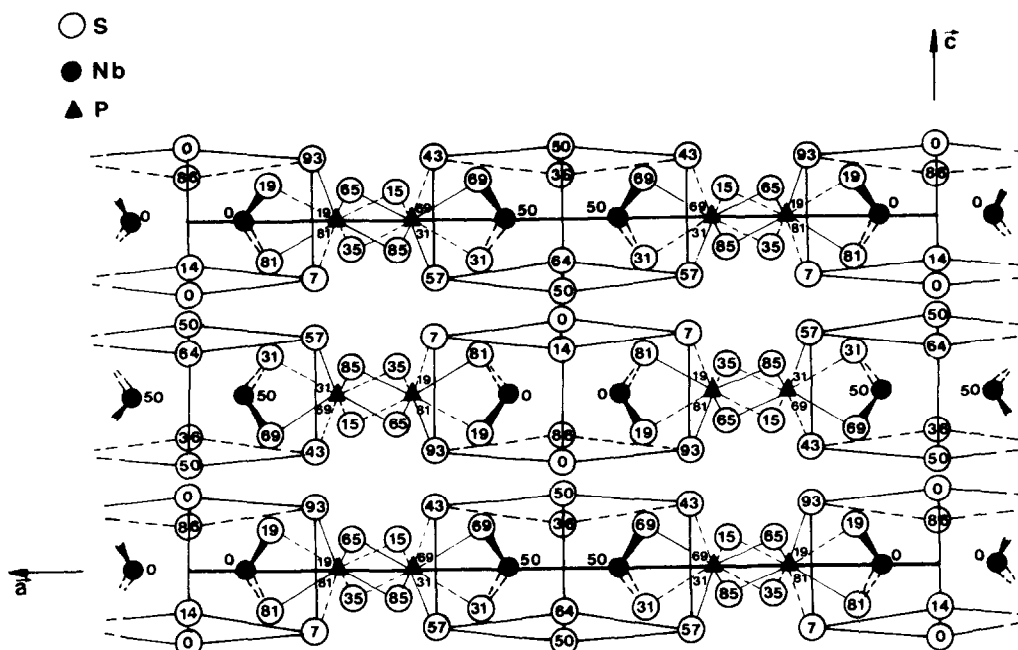
FIG. 3. Projection of 2D $P_2NbS_8$ along the $\vec{b}$ axis. Heavy continuous and dotted lines join the sulfur atoms constituting the niobium prismatic surrounding. Thin continuous and dotted lines join atoms of $(P_2S_6)$ groups. Numbers are fractional heights ($\times$ 100) of the atoms (*I*).

via interconnected $(PS_4)$ tetrahedra constituting $(P_4S_{12})$ rings (Fig. 4).

From interatomic-distance considerations one recognizes in both structures cage-shaped $(Nb_2(S_2)_2)$ units of approximately $D_{2h}$ symmetry so that these crystal structures can be described as follows:

2D—4 × $P_2NbS_8$

($D_{2h}$) special positions

$$= 2(Nb_2(S_2)_2) + 4(P_2S_6)$$
$$\quad\quad C_{2h} \text{ site} \quad\quad C_i \text{ site}$$

3D—4 × $P_2NbS_8$

($D_{2d}$) special positions

$$= 2(Nb_2(S_2)_2) + 2(P_4S_{12})$$
$$\quad\quad D_2 \text{ site} \quad\quad S_4 \text{ site}$$

First, the 12 internal vibrations of a $(Nb_2(S_2)_2)$ cage give rise to 24 modes at the center of the Brillouin zone of the crystal and they are classified under the irreducible representations of the $D_{2h}$ and $D_{2d}$ point groups, respectively:

2D $P_2NbS_8$

$$\Gamma^{D_{2h}} \text{cluster} = 3A_g + B_{2g} + B_{1g} + B_{3g} + A_u + B_{2u} + 2B_{1u} + 2B_{3u}$$

$$\Gamma^{C_{2h}} \text{site} = \quad\quad 4A_g \quad + \quad 2B_g \quad + \quad 2A_u \quad + \quad 4B_u$$

$$\Gamma^{D_{2h}} \text{crystal} = 4A_g + 4B_{2g} + 2B_{1g} + 2B_{3g} + 2A_u + 2B_{2u} + 4B_{1u} + 4B_{3u}$$
$$\quad\quad\quad\quad (R) \quad (R) \quad\quad (R) \quad\quad (R) \quad\quad — \quad\quad (IR) \quad\quad (IR) \quad\quad (IR)$$

## 3D $P_2NbS_8$

$$\Gamma^{D_{2h}} \text{ cluster} = 3A_g + A_u + B_{1g} + 2B_{1u} + B_{2g} + B_{2u} + B_{3g} + 2B_{3u}$$

$$\Gamma^{D_2} \text{ site} = 4A + 3B_1 + 2B_2 + 3B_3$$

$$\Gamma^{D_{2d}} \text{ crystal} = 4A_1 + 4B_1 + 3A_2 + 3B_2 + 5E$$
$$\phantom{\Gamma^{D_{2d}} \text{ crystal} =} (R) \quad (R) \quad - \quad (IR,R) \quad (IR,R)$$

One expects in the former case a splitting of the six Raman active modes into $(A_g + B_{2g})$ or $(B_{1g} + B_{3g})$ doublets. Similarly, $B_{1u}$- and $B_{3u}$-type modes must give rise to infrared doublets, while the $B_{2u}$ mode is no sensitive to correlation effects and the $A_u$ one becomes infrared active ($B_{2u}$ component). In the latter case, the infrared–Raman mutual-exclusion rule is removed, all the ungerade vibrations become Raman active, and coincidences are expected for $B_2$- and $E$-type crystalline vibrations. Finally, the
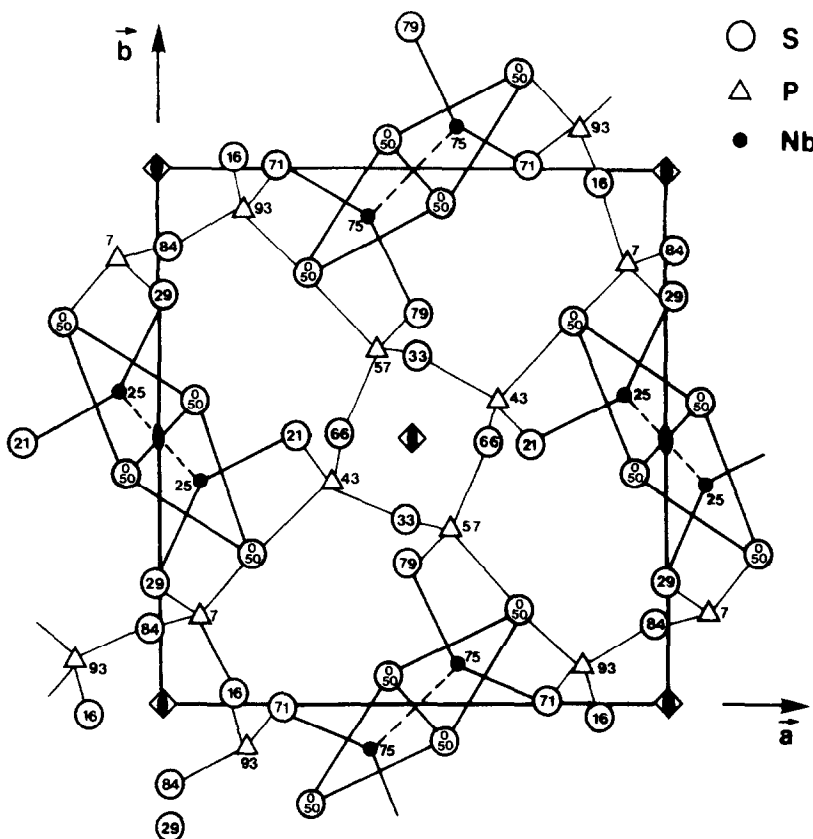


FIG. 4. Projection along the $\bar{b}$ axis of 3D-$P_2NbS_8$ tetragonal structure. Numbers are fractional heights ($\times$ 100) of the atoms (2).

three totally symmetric $A_g$ cluster modes should be split into $(A_1 + B_1)$ Raman doublets due to Davydov effects.

Concerning now the anionic fragments, the $(P_2S_6)^{2-}$ anion belongs also to the $D_{2h}$ point group symmetry, and its internal vibrations are classified according to the correlation diagram

$$\Gamma^{D_{2h}} (P_2S_6)^{2-} = 4A_g + 2B_{1g} + 2B_{2g} + B_{3g} + A_u + 3B_{1u} + 2B_{2u} + 3B_{3u}$$

$$\Gamma^{C_i} \text{ site} = \qquad\qquad 9A_g \qquad\qquad + \qquad\qquad 9A_u$$

$$\Gamma^{D_{2h}} \text{ crystal} = 9A_g + 9B_{1g} + 9B_{2g} + 9B_{3g} + 9A_u + 9B_{1u} + 9B_{2u} + 9B_{3u}$$
$$\quad\quad\quad (R)\quad\;\; (R)\quad\;\; (R)\quad\;\; (R)\quad\;\; -\quad\;\; (IR)\quad\; (IR)\quad\; (IR)$$

Thirty-six modes are Raman active and twenty-seven modes are infrared active, preserving mutual exclusion. The $(P_4S_{12})$ rings in the 3D compound are localized on $S_4$ symmetry sites and because of correlation effects, one obtains:

$$\Gamma^{S_4} (P_4S_{12}) = \qquad 11A \qquad + \qquad 11B \qquad + 10E$$

$$\Gamma^{D_{2d}} \text{ crystal} = 11A_1 + 11A_2 + 11B_1 + 11B_2 + 20E$$
$$\qquad\qquad\qquad (R)\qquad -\qquad (R)\quad\;\; (IR,R)\;\; (IR,R)$$

All the modes remain active and one expects a splitting of $B$-type vibrations into two Raman $(B_1 + B_2)$ components.

Finally, as far as lattice modes are concerned, in 2D $P_2NbS_8$ 18 librational vibrations are Raman active ($\Gamma_R^{D_{2h}} = 4A_g + 5B_{1g} + 4B_{2g} + 5B_{3g}$) and 15 translational motions are infrared active ($\Gamma_T^{D_{2h}} = 4A_u + 4B_{1u} + 3B_{2u} + 4B_{3u}$) excluding the acoustic modes. In contrast, Raman and infrared coincidences are expected in the low-frequency spectra of the 3D compound ($\Gamma_R^{D_{2h}} = A_1 + 2A_2 + B_2 + 4E$ and $\Gamma_T^{D_{2d}} = A_1 + B_1 + B_2 + 3E$).

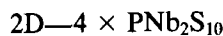## 2D $PNb_2S_{10}$ and 2D $P_2Nb_4S_{21}$

The layered $PNb_2S_{10}$ compound crystallizes with orthorhombic symmetry, space group $P2_12_12 (D_2^3)$, with four entities per unit cell, and the 2D $P_2Nb_4S_{21}$ crystal shows the monoclinic symmetry space group $C2/c$ ($C_{2h}^6$), with two entities per primitive unit cell.

In these compounds, the $(Nb_2S_{12})$ units are directly linked to each other not only through $S \cdots S$ edges of the prisms but also through one of their bicapping sulfur atoms, forming infinite $(Nb_2S_9)$ chains (Fig. 5). It is noteworthy that the capping sulfur is also involved in a S—S bond with one of the edge sulfur atoms, and it gives rise to a new $S_2^{2-}$ pair (intercluster pair). In the first $PNb_2S_{10}$ compound, bonding between the chains takes place through $(P_2S_8)$ units built of two $(PS_4)$ groups, i.e., two $(PS_3)$ groups sharing again another $S_2^{2-}$ pair (intraanionic pair). In the second case of $P_2Nb_4S_{21}$, the chains are linked to each other through $(P_2S_9)$ units made from two $(PS_4)$ tetrahedra themselves interacting with an extra sulfur atom, i.e., two $(PS_3)$ groups sharing a $(S_3)^{2-}$ anionic group (3, 4).
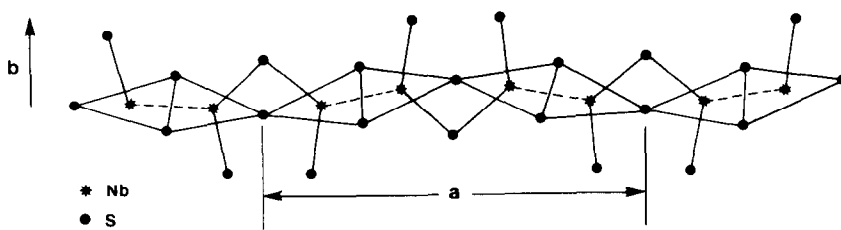
FIG. 5. Schematic representation of a $(Nb_2S_9)$ infinite chain.

In both compounds, as previously mentioned for $P_2NbS_8$ phases, the distances between niobium and sulfur atoms constituting the common rectangular face of the biprism are shorter than the other Nb–S distances ($\sim 2.55$–$2.59$ Å as compared with $2.47$–$2.54$ Å); nevertheless, $(Nb_2$–$S_2^{2-})$ interactions involving intercluster pairs are still very strong. This implies that "isolated" $(Nb_2(S_2)_2)$ clusters cannot be considered, and we propose to describe the molecular structures according to the following formulae:

2D—4 × $PNb_2S_{10}$

$D_2^3$ special positions

$\quad = 4(Nb_2(S_2)_2S_2) + 2(P_2S_6(S_2))$
$\qquad\quad C_1$ site $\qquad\quad C_2$ site

2D-2 × $P_2Nb_4S_{21}$
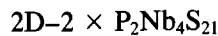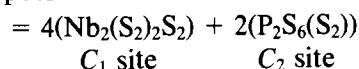
$C_{2h}^6$ special positions

$\quad = 4(Nb_2(S_2)_2S_2) + 2(P_2S_6(S_3))$
$\qquad\quad C_1$ site $\qquad\quad C_i$ site
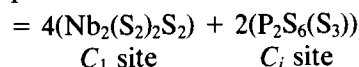
Consequently, the correlation diagrams between site and factor groups for the anionic frameworks are:

$(P_2S_6(S_2))$

$\Gamma^{C_2}$ site $= \quad 13A \quad + \quad 11B$

$\Gamma^{D_2}$ crystal $= 13A_1 + 13B_1 + 11A_2 + 11B_2$
$\qquad\qquad\quad$ (R) $\quad$ (IR,R) $\quad$ (IR,R) $\quad$ (IR,R)

$(P_2S_6(S_3))$

$\Gamma^{C_i}$ site $= \quad 12A_g \quad + \quad 15A_u$

$\Gamma^{C_{2h}}$ crystal $= 12A_g + 12B_g + 15A_u + 15B_u$
$\qquad\qquad\qquad$ (R) $\quad$ (R) $\quad$ (IR) $\quad$ (IR)

It is noteworthy that, in the $P_2Nb_4S_{21}$ structure, a dynamical disorder of the central S atom in $(S_3)^{2-}$ catenated anions can only account for the time averaged special centrosymmetric positions of the anionic fragments (4).

Similarly, correlation tables for the vibrations of the complex $(Nb_2(S_2)_2S_2)$ units can be established, and in both cases one expects complex spectra with many Raman and infrared coincidences.

Finally, in the low-frequency regions, chain-bending vibrations and also lattice modes will be expected and only tentative assignments can be suggested.
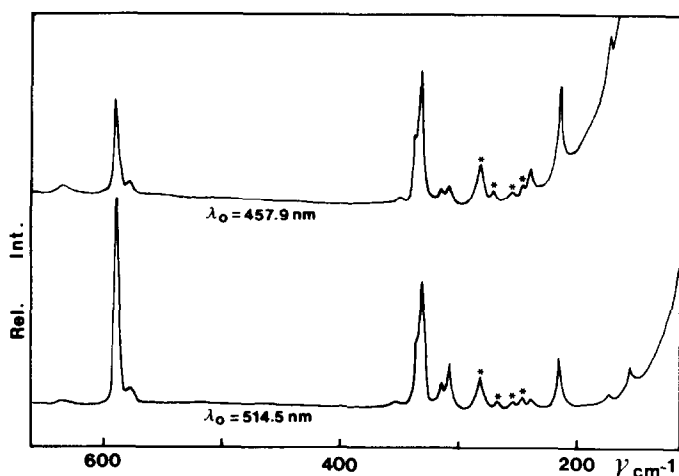
FIG. 6. Raman spectra (650–100 cm$^{-1}$) of a polycrystalline sample of $NbS_2Cl_2$ at 300 K using two different exciting lines. (*) Bands assigned to $\nu Nb$–Cl vibrations.

## Vibrational Results and Discussion

Raman spectra of powdered samples of $NbS_2Cl_2$ using the 514.5 and 457.9 nm exciting lines are shown on Fig. 6. The infrared and Raman ($\lambda_0$ = 514.5 and/or 488.0 nm) spectra for polycrystalline samples of 2D $P_2NbS_8$, 3D $P_2NbS_8$, 2D $PNb_2S_{10}$, and 2D $P_2Nb_4S_{21}$ are shown in Figs. 7, 8, 9, and 10, respectively. The corresponding band positions and proposed assignments are re-ported in Tables I–III. Finally, the UV-visible absorption spectra of the four P–Nb–S solid phases under study are shown on Fig. 11.

### Vibrational Spectra of $NbS_2Cl_2$

The vibrational spectra of $NbS_2X_2$ compounds ($X$ = Cl, Br, I) have been already reported by Perrin et al. (10, 11), but in-complete Raman data were obtained be-
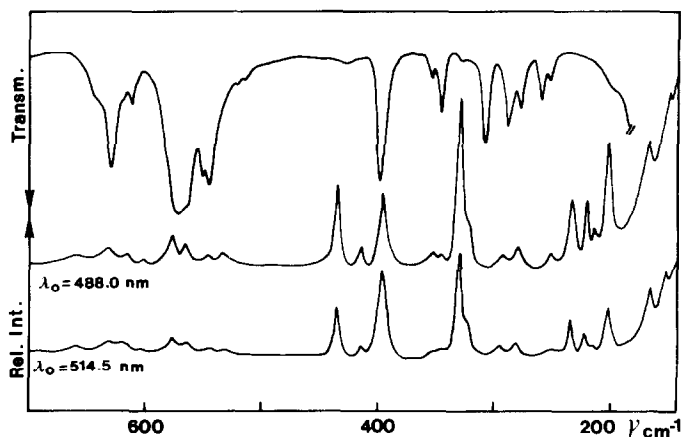


FIG. 7. Infrared and Raman spectra (700–100 cm$^{-1}$) of 2D $P_2NbS_8$ at 300 K.
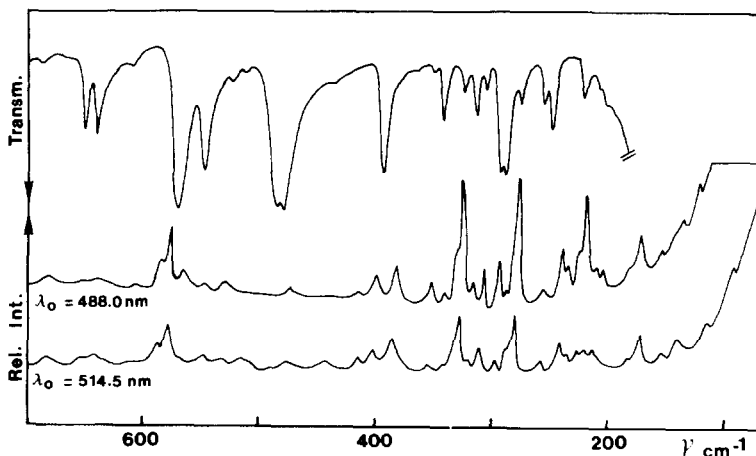
FIG. 8. Infrared and Raman spectra (700–100 cm⁻¹) of 3D $P_2NbS_8$ at 300 K.

cause of photodecomposition of the samples under the He–Ne ($\lambda_0 = 632.8$ nm) laser beam. Such effects were avoided in this study even when using different exciting lines from 514.5 and 457.9 nm.

We have observed all the expected Raman modes and in particular we assign the three intense bands at 590, 332, and 214 cm⁻¹ to the totally symmetric $A_g$ vibrations, namely, $\nu S–S$, $\nu_s Nb–(S_2)_2$, and $\nu Nb–Nb$ (Fig. 6). The last mode, not observed in Ref. (10), was erroneously identified with a

plasma line at ~188 cm⁻¹. As far as the $\nu_a Nb–S_2$ ($M_5$ mode) and deformation cluster vibrations are concerned, we assign the new weak signal at 354 cm⁻¹ to $M_5$ (its infrared out-of-phase counterpart, $M_8$, has been previously observed at 377 cm⁻¹) and we locate $M_6$ ($B_{3g}$) and $M_4$ ($B_{1g}$) vibrations at ~310 and ~240 cm⁻¹, respectively. The additional bands in the frequency range 300–240 cm⁻¹ correspond to intercluster $\nu$Nb–Cl vibrations in agreement with infrared results for $NbS_2Cl_2$ (10) and $Nb_2Cl_{10}$ (13).



FIG. 9. Infrared and Raman spectra (700–100 cm⁻¹) of 2D $PNb_2S_{10}$ at 300 K.

TABLE I

INFRARED AND RAMAN BAND POSITIONS (cm⁻¹) IN 2D $P_2NbS_8$ AND COMPARISON WITH VIBRATIONAL DATA FOR $NbS_2Cl_2$, $Ag_2P_2S_6$, $Tl_2P_2S_6$, AND $Al_2Cl_6$ AT 300 K

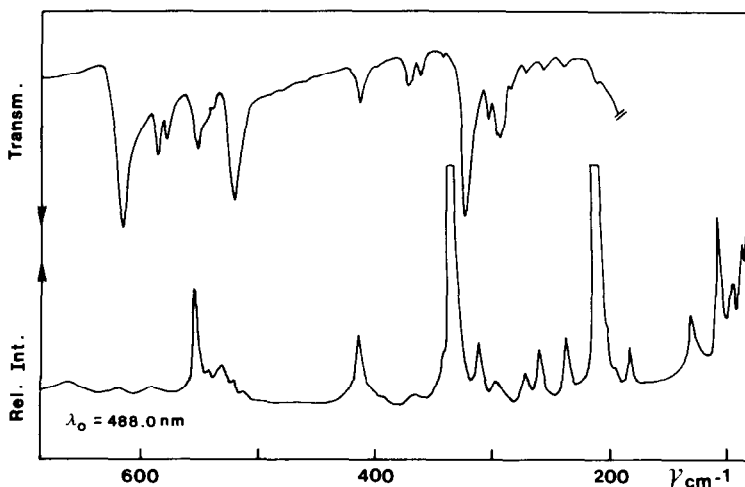| $Al_2Cl_6$ (20) | | $Tl_2P_2S_6$ (18, 19) | | $Ag_2P_2S_6$ (17) | | 2D $P_2NbS_8$ | | | $NbS_2Cl_2^b$ |
|---|---|---|---|---|---|---|---|---|---|
| IR | Raman | IR | Raman | IR | Raman | IR | Raman | Tentative assignments$^a$ | IR $M_i$ Raman (sym.) |
| | | | | | | | 830 vw | $435 + 397 = 832$ cm⁻¹ | |
| | | | | | 795vw | | 790vw | $2 \times 397 = 794$ cm⁻¹ | |
| | | 665w | 731vw (C) | | 786vw | | 763w | $435 + 329 = 764$ cm⁻¹ | |
| | | | | | | [737sh | | $397 + 347 = 744$ cm⁻¹ | |
| | | | | | | 721m.br] | 725w | $398 + 325 = 723$ cm⁻¹ | |
| | | | | | | | 657w ↗ | $397 + 329 = 726$ cm⁻¹ | |
| | | | | | | | | $2 \times 329 = 658$ cm⁻¹ | |
| 622 ($\nu_8$) | | 640s ($\nu_8$) | | 614s / 592m ($\nu_8$) | | 643sh,m / 628s | 628s | $\nu_8 + \nu_{11}:\nu_4 PS_2^{term}$ | 590s / 580w   $M_1$ (Ag) |
| | 604 ($\nu_{11}$) | | [645w / 612vw] ($\nu_{11}$) | | [641w / 612w] ($\nu_{11}$) | [618sh / 610m] | 613vw / 602vvw | $+ (329 + 281 = 610$ cm⁻¹$)$ | |
| | 520 ($\nu_1$) | | 592m ($\nu_1$) | 580m | [577m / 554w] ($\nu_1$) | [570vs / 562sh] | 573m / 563w | $\nu_1:\nu_s PS_2^{term} + M_1 + M_{11}$ | 588s / 582sh   $M_{11}$ ($B_{3u}$) |
| | | 540w (C) | | 556w / 542m | | 551s / 545s | | | |
| | | | | | | | [545vw] / 531w,br ↗ | $\nu_{16}:\nu_s PS_2^{term}$   $+ (329 + 203 = 532$ cm⁻¹$)$ | |
| 482 ($\nu_{16}$) | | 530m ($\nu_{16}$) | (C) | 520s | [521w / 514w] ($\nu_{16}$) | 521vvw / 514vw | | | |
| | | | 492w (C) | | 498w / 474w (C) | | | | |
| 426 ($\nu_{13}$) | | 480m,br ($\nu_{13}$) | | 466m / 454sh / 428vw ($\nu_{13}$) | | 456vw | | $\nu_{13}$ | |
| | 347 ($\nu_2$) | 420m | 415vs ($\nu_2$) | | 418vs ($\nu_2$) | | 435s / 414m | $\nu_2$   ($\nu^{bridg.}$) | |
| 322 ($\nu_{17}$) | | 392m-s ($\nu_{17}$) | (C) | 395w ($\nu_{17}$) | | [400vs / 398sh] | | $\nu_7$ | 377m   $M_8$ ($B_{1u}$) |
| | 289 ($\nu_6$) | | 395vw / 365m / 360vw ($\nu_6$) | | 398s / 370vw / 362vw ($\nu_6$) | | 397s | $\nu_6$   $M_8 + M_5$ | $M_5$ ($B_{2g}$) |
| | | 360vw / 345m-s | | | | 356m / 347s / [327vw] | 352w / 346vw / 329vs ↗ / 325sh | $M_2$ | 362vs   $M_{10}$ ($B_{2u}$)   354vw |

(The central assignment column also shows a drawn structure of the bridged $P_2S_2$ ring, labelled $\nu^{bridg.}$, between the entries for $\nu_{13}$, $\nu_2$, $\nu_7$, and $\nu_6$.)

| ν (P₂S₆) | | | | | Assignment | | Cluster mode |
|---|---|---|---|---|---|---|---|
| ν₃ | 175 | ν₃ 221 | ν₃ 304s | ν₃ 299m | 312sh, 310s | 294vw  ν₃:δPS₂^term  M₁₀ | 323vs | M₂ (A_g) {337sh, 332s} |
| | | | | | | | M₉(B₁u), M₁₂(B₃u)? |
| | | | | | 289s, 278m | 281m  M₉ | M₆ (B₃g) {315sh, 309m} |
| ν₉ | 142 | ν₉ and/or ν₁₈  249m-s | | ν₉+ν₁₈  259m | 262m | 262w  ν₉:rock. PS₂ and/or | M₁₂ + M₆ |
| ν₁₈ | | | | ν₉+ν₁₈ | 254m | [253vw]  ν₁₈:δPS₂^term | 295vs  ν Nb–Cl {282m, 275sh} |
| | | | | | | 235m  ν₇:wag. PS₂  M₄ | M₄ (B₁g) {255sh, 250vs, 245sh, 218w} 255vw, 246vw, 240w  ν Nb–Cl |
| ν₇ | 162 | ν₇ 244s | ν₇ 247w | ν₇ 233m | | 222m ↗ | |
| | | 226vs, 218vw | 226w | 219vw | [202vw] | 203vs  ν₁₅:twist PS₂ and/or  M₃ | M₃ (A_g) 214m |
| ν₁₅ | 160 | 200vw | 210w | | | 216w | |
| | | ν₁₅+ν₄ {196m, 175vs} | ν₁₅+ν₄ {206m, 200m} | | | 169m | |
| ν₄ | 107 | | | | | | |
| ν₁₄ | 135 | ν₁₄ 189m-s | ν₁₄ 184m | | 181w | ν₁₄:wag. PS₂ or M₇ | 166s  M₇ (A_u) |
| ν₁₂ | 122 | ν₁₂ 159s | ν₁₂ 141m | | | ~154w  ν₁₂:rock. PS₂ or R' cluster | Def Nb–Cl {172vw, 154w} + R' cluster |
| ν₅ | ~78 | 122vw | 120m, 90m | | | | |
| ν₁₀ | ~42 | ν₁₀ 60m | | | | | |
| | | T'_T1 + lattice modes {75, 48} | T'_Ag + lattice modes {75m, 62w, 50s, 41w, 32m, 22w} | | | | |
| lattice modes | | 29 | 31vw | | | | |

ν₄,δ

P / S ... P / S (bridge structure)

---

FIG. 10. Infrared and Raman spectra (650–100 cm$^{-1}$) of 2D $P_2Nb_4S_{21}$ at 300 K; arrows indicate bands assigned to $S_3^{2-}$ vibrations (see text).

Finally, the low-frequency Raman signals at 172 and 154 cm$^{-1}$ probably come from $\delta NbCl_2$ bending vibrations and/or librational cluster motions. In order to check these assignments, several Raman spectra were recorded using exciting radiations ranging from 514.5 to 457.9 nm, and intensity variations were estimated with respect to the 465 cm$^{-1}$ band of $KClO_4$ used as internal standard. However, as the laser incident energy increases, no drastic intensity enhancements were observed and, in con-trast, the intensity of the $\nu S-S$ band at 590 cm$^{-1}$ decreases markedly. This may be due in part to the strongly absorbing nature of this semiconductor-type material which exhibits an absorption edge at ~320 nm and an intense electronic transition at 365 nm (14); also, antiresonance phenomena or interference effects between low lying Laporte-forbidden $d–d$-type transitions and higher energy allowed transitions can be invoked (15, 16). In fact, according to photoelectron results and atomic orbital studies



FIG. 11. UV-Visible absorption spectra of 2D and 3D $P_2NbS_8$, 2D $PNb_2S_{10}$, and 2D $P_2Nb_4S_{21}$ at 300 K (wavelengths of some maxima are reported).

## TABLE II

INFRARED AND RAMAN BAND POSITIONS (cm$^{-1}$) IN 3D $P_2NbS_8$ AND COMPARISON WITH VIBRATIONAL DATA FOR $P_4S_{10}$ AND $Ag_4P_2S_7$ AT 300 K

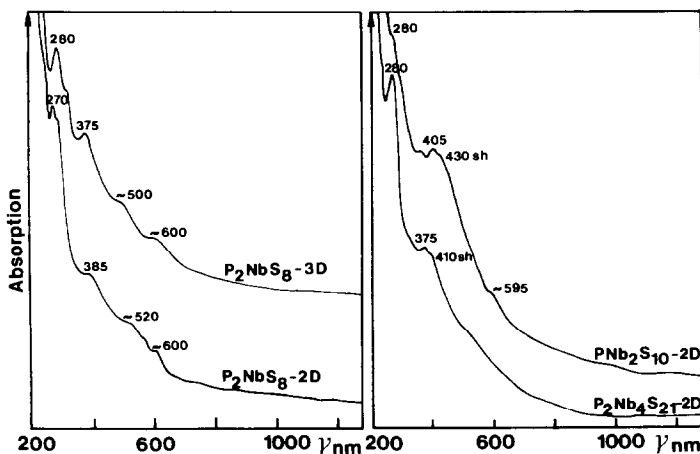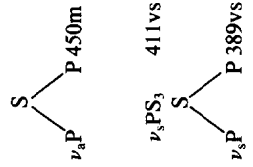| $P_4S_{10}$ (21) | | $Ag_4P_2S_7$ (17) | | 3D $P_2NbS_8$[a] | | |
|---|---|---|---|---|---|---|
| IR | Raman | IR | Raman | IR | Raman | Tentative assignments |
| | | | | 803w | | $481 + 328 = 809$ cm$^{-1}$ |
| | | | | 738sh | | $396 + 346 = 742$ cm$^{-1}$ |
| | | | | 721m,br | | $396 + 328 = 724$ cm$^{-1}$ |
| 715vw | 715m-s | | | 689vw | 681vw | $396 + 296 = 692$ cm$^{-1}$ |
| 690vs | 689m | | | 651s | 649vw | } $\nu_a PS_2$ term |
| 650m-w | 656w | | | 640s | 641vw | |
| | 640vw | | | 612vw | 611vw | $328 + 281 = 609$ cm$^{-1}$ |
| | | 596m | 601w | | 584sh | $\nu_s PS_2$ term |
| | | 570m | | 571vs | 578m | $+ M_1 + M_{11}$ |
| 565vw | 560vw | 540sh } $\nu_a PS_3$ { | 550w | 566sh | 565w | |
| | | 526s | | 549s | 548vw↗ | $328 + 222 = 550$ cm$^{-1}$ |
| | | 512s | 504m | 527w | 528w | } $\nu_s PS_2$ term |
| | | | | 516vw | 517vw | |
| 530vs | 530vw | | | 487vs | | S / $\nu_a$P \ P |
| | 486vw | 454s  $\nu_a$P—P  450m | | 481vs | 476w | |
| 410sh | 480sh | | | | 459vw | |
| 390w | 398m | 405m  $\nu_s PS_3$  411vs | | 440vw | 440w | |
| | | | | | 412w | |
| | | | 389vs ($\nu_s$P—P) | 396s | | |
| | | | | | 400s | S / $\nu_s$P \ P |
| | | | | 371vw | 384m | |
| | | | | 354vw | 353m | $M_8 + M_5$ |
| | | | | 346m | 343vw | |
| | | | | | 332sh | |
| | | | | [328m] | 328s↗ | $M_2$ |
| | | | | 318m | 318w | $\delta$P—P or $\delta S_2$—S |
| | | | | 310m | 309m | $M_{10}$ |
| | | | | 296s | 296m | } $\delta PS_2 + M_9$ |
| | | | | 292s | 290vw | |
| | | 298w | 285m | 280m | 281s↗ | $M_{12} + M_6$? |
| 267sh | 272s | 283m  $\delta PS_3$ | | 260m | 258w | } r. $PS_2$ |
| 264m | | 275w   + | 255m | 251s | | and/or $\delta PS_2$ |
| 260sh | 260sh | 250vw   $\delta$ | | | 243w | } w.$PS_2$ |
| | | 225vw  S  210s | | | 238m | |
| 205sh | 203sh | | | [225m] | 228w↗ | } $M_4 + M_3$ |
| 192sh | 198vs | | | | 222s↗ | |
| 189w | 188m | | | 213vw | 213m | tw. $PS_2$ and/or $\delta$P—P |
| 162vw | 160m | | | 206vw | 207m | $\delta P_4 S_{12}$ |
| | | | | | 182w | w. $PS_2$ and/or $M_7$ |
| | | | 176w | 171m | | tw. $PS_2$ and/or $\delta$P—P |
| | | | | 153vw | | r. $PS_2$ or $R'$ cluster? |
| 130sh | 138m | | | 136m | | } bending ($P_4S_{12}$) |
| 124s | 132sh | | | | 120w | |
| | | | | | 93w | |
| | | | | | 70w | |

$^a$ Same symbols as in Table I.

TABLE III

Infrared and Raman Band Positions (cm⁻) in 2D $PNb_2S_{10}$ and 2D $P_2Nb_4S_{21}$ and Comparison with Vibrational Data in $Ag_4P_2S_7$ at 300 K

| $P_2Nb_4S_{21}{}^a$ | | | $Ag_4P_2S_7$ (17) | | $PNb_2S_{10}{}^a$ | | |
|---|---|---|---|---|---|---|---|
| IR | Raman | Tentative assignments | IR | Raman | Raman | IR | Tentative assignments |
| | 656vw,br | $2 \times 331 = 662$ cm⁻¹ | | | 664w,br | 622sh | $2 \times 332 = 664$ cm⁻¹ |
| 610vs | 612vw | $\Big\}\,\nu_a PS_3$ | 596m | 601w | 662vw,br | 611vs | |
| 580m | 584vw | | 570m | | 591vw | 582m | $\Big\}\,\nu_a PS_3$ |
| 575m | | | | | | 573m | |
| 564w | 563m-w | $M_1 + M_{11}$ intracluster | 540s | 550w | 556m | 550sh | $M_1 + M_{11}$ intracluster |
| | 559m-w | $\nu S_2^{2-}$ intercluster | 526s | | 540sh | 547m | $\nu S_2^{2-}\begin{cases}\text{intercluster}\\\text{intra-anionic}\end{cases}$ |
| 541w | 544m-w | $+ (331 + 203 = 534$ cm⁻¹$)$ | | | 535w | 540sh | $+ (332 + 208 = 540$ cm⁻¹$)$ |
| 532w | 531w | | | | | 535w | |
| 521m | 521vw | $\Big\}\,\nu'_a PS_3$ | 512s | 504m | 520vw | 516vs | $\Big\}\,\nu'_a PS_3$ |
| 514vs | 506vw | | | | 508vw | | |
| 491vw | | | | | | | |
| 455m-w | 462vw | (b) $\nu_a + \nu_s S_3^{2-}$ | 454s | $\nu_a P \angle S \quad$P 450m | | | |
| | 424m-w | | | | | | |
| 409m-w | 411m | $\Big\}\,\nu_s PS_3$ | 405m | 411vs | 415m | 410m | $\nu_s PS_3 + (2 \times 208 = 416$ cm⁻¹$)$ |
| 405m | | | | $\nu_s P \angle S \quad$P 389vs | 406w | | |
| | | | | | 395vw | | |

| Column 1 | Assignment (1) | Column 2 | δPS₃ + δP structure | Column 3 | Column 4 | Assignment (4) |
|---|---|---|---|---|---|---|
| 366m / [342w] / 345m-w | $M_8 + M_5$ | | | 370m / 366m / 358m | 364vw | $M_8 + M_5$ |
| [333sh] / 331vs | $M_2$ | | | [345vvw] / [339vw] | 342w / 332vs | $M_2$ |
| 320w | $M_{10}$ | | | 318vs | 311m | $M_{10}$ |
| 329s / 325sh | $\nu$Nb–S₂ (intercluster) | | | | | $\nu$Nb–S₂ (intercluster) |
| 295s / 290sh / [292vw] / [286vw] | $M_9$ | 298w / 283m / 275w | $\delta$PS₃ + $\delta$P, S–P structure: 285m, 255m P; 250vw / 225vw; 210s | 301m / 292m / 289m / 281w | [295w] | $\delta$PS₃ + $M_9$ |
| 282m / 278vvw | | | | | | |
| [262w] / [252w] / 238w | $\delta$PS₃ + $M_{12}$ + $M_6$ + $M_4$ | 262w / [247vw] / [234w] | | 268w / 254w / 237w | 272m / 259m / 236w | $M_{12}$ + $M_6$ + $M_4$ |
| 227vw | $\delta$S₃²⁻ [b] | | | | | |
| 203vs / [201vw] | $M_3$ | 227vw / 203vs | | 209w | 208vs / 204sh | $M_3$ |
| 174w | $M_7$ | 174w / 176w | | | 194vw / 181m-w | $M_7$ |
| 153w / 141w / 125w | chain bending | | | | 127m / 103m | R' and T' cluster |
| 118vw / 108m-w / 95m-w / 71sh | | | | | 90vw / 81w / 74sh / 66vw | chain bending |

[a] Same symbols as in Table I.

[b] Bands observed at 476, 458, and 227 cm⁻¹, respectively, in BaS₃ (24).

carried out by Bullet (*12*) and Rijnsdorp (*8*) on the ($Nb_2(S_2)_2$) cage, the highest filled level and the next unoccupied molecular orbitals are composed of ~90% niobium *d* states, the last occupied $Nb-4dz^2$ ($A_g$ symmetry) bonding orbital lying just above the highest occupied $S-3p_y^*$ ($B_{1g}$ symmetry) orbital. We thus attribute the high-energy transition at ~365 nm to a vibronically allowed metal-to-ligand charge-transfer transition. Now, if we compare both spectra displayed in Fig. 6, we can use the $\nu Nb-Cl$ band at ~282 $cm^{-1}$ as an internal standard which takes into account absorption effects, in which case we note mainly intensity disenhancements of $\nu S-S$ ($A_g$), and $B_{2g}$- and $B_{3g}$-type modes, while some apparent enhancements are observed for the remaining bands, in particular those assigned to the $\nu_s Nb-(S_2)_2$ and $\nu Nb-Nb$ ($A_g$) vibrations. These preliminary results under preresonance conditions thus confirm not only our proposed assignments of the low-frequency totally symmetric modes but also the electric-dipole-allowed character of the high-energy charge-transfer transition. Moreover, since the four P–Nb–S phases under study exhibit also a strong electronic transition at ~375–405 nm (see below), we have recorded their Raman spectra with different excitations in order to detect similar Raman intensity disenhancements.

*Vibrational Spectra of 2D $P_2NbS_8$*

In conjunction with spectroscopic data concerning the $(P_2S_6)^{2-}$ ion in $Ag_2P_2S_6$ (*17*) or $Tl_2P_2S_6$ (*18, 19*) and the isoelectronic $Al_2Cl_6$ molecule (*20*), the above results for $NbS_2Cl_2$ allow us to propose complete assignments of the vibrational spectra of 2D $P_2NbS_8$ (Table I).

First, most of the cluster modes appear as well-resolved doublets or as asymmetric signals in agreement with crystal-effect expectations and they are generally shifted toward lower frequency values (−10 and −30 $cm^{-1}$). We assign the very broad and intense absorption band at 570 $cm^{-1}$ to the

$\nu S-S$ $B_{3u}(M_{11})$ mode and the corresponding Raman-active symmetric ($M_1$) mode must surely contribute to the medium intensity doublet at 573–563 $cm^{-1}$. The strong Raman bands at 329 and 203 $cm^{-1}$ are assigned to other $A_g$ vibrations, namely, $\nu_s Nb-(S_2)_2$ and $\nu Nb-Nb$, while the infrared-active out-of-phase stretching $B_{2u}$ mode gives rise to an intense doublet at ~310 $cm^{-1}$. At higher frequencies, the strong infrared doublet at 356–347 $cm^{-1}$ and its weaker Raman counterpart a 352–346 $cm^{-1}$ are attributed to $\nu_a Nb-S_2$ $M_5$ and $M_8$ modes, respectively. Finally, the two medium absorption bands at 289 and 278 $cm^{-1}$ and the Raman signal at 281 $cm^{-1}$ can be assigned to $M_9$, $M_{12}$, and $M_6$ cluster fundamentals since no vibrational modes of the $(P_2S_6)^{2-}$ entities are expected in this frequency range. The last $B_{1g}$-type ($M_4$) cage vibration is tentatively located at 222 $cm^{-1}$. It is noteworthy that this last mode and the two totally symmetric $\nu_s Nb-(S_2)_2$ and $\nu Nb-Nb$ vibrations undergo apparent Raman intensity enhancements when changing the exciting line from 514.5 to 488.0 nm (Fig. 7). This preresonance Raman result reflects again the charge-transfer character of the dipole-allowed electronic transition observed at ~385 nm (Fig. 11).

As far as vibrations of ($P_2S_6$) units are concerned, the vibrational spectra of 2D $P_2NbS_8$ show remarkable similarity with those of $Ag_2P_2S_6$ (*17*) and $Tl_2P_2S_6$ (*18, 19*). As shown in Table I, assignments of the three compounds can be established simultaneously and frequency values can be compared, while large frequency shifts due to mass effects are noted for the isoelectronic $Al_2Cl_6$ molecule (*20*). We thus propose some new assignments for $Tl_2P_2S_6$, in disagreement with the results published by Wibbelmann *et al.* (*18*).

In the high-frequency region (850–650 $cm^{-1}$) numerous weak bands are observed and explained in terms of overtones and combinations. Several sets of intense infrared bands and weak Raman signals at ~630,

610, 570, and 520 cm$^{-1}$ are assigned to stretching vibrations of the terminal (PS$_2$) groups (involved in weaker Nb $\cdot\cdot\cdot$ S interactions) while the stretching modes of bridged P$\overset{\displaystyle S}{\diagup\diagdown}$P bonds are easily identified with strong signals in the range 440–390 cm$^{-1}$. Only the bands due to $\nu$PS$_2$ modes show some crystal splittings, but we have never observed all the theoretically expected components, which confirms, in agreement with X-ray data (*1*), that (P$_2$S$_6$)$^{2-}$ anions are weakly interacting. Now, the infrared doublet at 262–254 cm$^{-1}$ is attributed to the overlapping $\nu_9$ (rock. PS$_2$) and $\nu_{18}$ ($\delta$ PS$_2$) vibrations, and the strong Raman bands at 235 and 169 cm$^{-1}$ are assigned to $\nu_7$ (wag. PS$_2$) and $\nu_{15}$ (twist. PS$_2$) modes, with an expected strong contribution of the $\delta$ P$\overset{\displaystyle S}{\diagup\diagdown}$P deformation. In the low-frequency region, only tentative assignments are proposed. The weak infrared and Raman bands at 181 and 154 cm$^{-1}$, respectively, may be due either to a bending vibration of (PS$_2$) groups or to deformation (or librational) motion of (Nb$_2$(S$_2$)$_2$) cages.

Finally, in agreement with the above selection rules, it may be pointed out that these spectra exhibit quite a few infrared and Raman coincidences as indicated by band positions with brackets in Table I. We thus conclude that the main interatomic interactions are effective within both (Nb$_2$(S$_2$)$_2$) and (P$_2$S$_6$) frameworks.

*Vibrational Spectra of 3D P$_2$NbS$_8$*

The spectra of 3D P$_2$NbS$_8$ show the same general pattern as previously observed for the 2D derivative and one recognizes again modes due to the (Nb$_2$(S$_2$)$_2$) unit in addition to bands due to the anionic fragment. However, at first glance the spectra are more complex and structured (Fig. 8), a result in agreement with the selection rules which predict that all the vibrations become Raman active. First of all, some relative intensity changes are noted for the cluster modes. The $\nu$S–S stretching vibrations of S$_2^{2-}$ pairs give rise to a very strong asymmetric infrared band at ~570 cm$^{-1}$ and to a Raman doublet at 578–565 cm$^{-1}$; these positions compare favorably with those previously found, since the S–S bond lengths are nearly equivalent (2.014 Å compared to 2.024 Å). The two $A_g$ vibrations, $\nu_s$Nb–(S$_2$)$_2$ at 328–332 cm$^{-1}$ and $\nu$Nb–Nb at 222–228 cm$^{-1}$, again show Raman intensity enhancements under preresonance conditions when the laser energy approaches that of the intense charge-transfer electronic transition at 375 nm (Fig. 11). However, care must be exercised in discussing a selective enhancement mechanism since intensities of all the cluster modes have apparently increased when changing the exciting radiation from 514.5 to 488.0 nm. We thus conclude that a strong distortion and a lowering of symmetry of the cages have taken place. Several infrared and Raman coincidences were indeed observed, although this was not expected for the totally symmetric $A_g$ modes (Table II).

To propose assignments of the (P$_4$S$_{12}$) ring frequencies, we have made use of spectroscopic data already known for the P$_4$S$_{10}$ molecule (*21*) and the (P$_2$S$_7$)$^{4-}$ ion (*17*), which present sulfur bridged P$\overset{\displaystyle S}{\diagup\diagdown}$P bonds. Four main regions with several sets of peaks showing infrared–Raman coincidences can be distinguished:

(i) In the high-frequency regions 650–610 cm$^{-1}$ and 580–510 cm$^{-1}$, the bands are assigned to $\nu_a$PS$_2$ and $\nu_s$PS$_2$ vibrations of terminal (or "extracyclic") P–S bonds.

(ii) In the range 490–370 cm$^{-1}$, several new and intense (infrared) bands are observed which must take origin from stretching vibrations of "endocyclic" P$\overset{\displaystyle S}{\diagup\diagdown}$P bridged bonds.

(iii) Below 320 cm$^{-1}$, the PS$_2$ bending modes occur and the corresponding frequencies follow the same pattern as for 2D

$P_2NbS_8$. However, two additional bands appear at 318 and 213 cm$^{-1}$ and are tentatively

assigned to $\delta$ P $\overset{S}{\underset{}{\quad}}$ P deformation.

(iv) Finally, some low-frequency ($\nu \leq 150$ cm$^{-1}$) and weak Raman signals are observed which probably come from deformation and librational motions of ($P_4S_{12}$) rings with likely contributions of intermolecular cluster modes.

We thus emphasize that precise and complete assignments of these spectra are not straightforward; however, it is obvious that 2D and 3D $P_2NbS_8$ compounds can be easily characterized by their quite different vibrational spectra.

## Vibrational Spectra of 2D $PNb_2S_{10}$ and 2D $P_2Nb_4S_{21}$

In these compounds, we have previously mentioned that a description of a part of the crystal structures in terms of isolated ($Nb_2(S_2)_2$) cages was a crude approximation. Nevertheless, such a model seems to apply again, since we observe all the bands yet assigned to ($Nb_2(S_2)_2$) cluster modes at very close frequency values. This means that intercluster vibrational couplings within the infinite chains are weak, a result in agreement with the low multiplicity of the detected signals (no further splittings were observed by cooling the samples down to 80 K). Moreover, as the spectra of both compounds show a great similarity, we conclude that short-range interactions of the same order of magnitude are taking place in between the ($Nb_2S_9$) chains of these layered systems.

As expected, most of the cage vibrations are both infrared and Raman active. First, the intracluster $\nu$S–S vibrations are localized at 560–550 cm$^{-1}$, i.e., at lower frequencies than in 2D $P_2NbS_8$, in agreement with X-ray data which have converged to significantly larger $d$(S–S) distances (2.043 Å as compared with 2.024 Å). The several peaks observed between 565 and 535 cm$^{-1}$ can thus be assigned according to the different

S–S bond lengths found in the crystal structures (ranging from 2.041 to 2.066 Å). In addition, the more complex infrared spectrum of $PNb_2S_{10}$ in this region is probably due to the existence of a third type of $S_2^{2-}$ pairs within the ($P_2S_6(S_2)$) units. These assignments (Table III) are supported by empirical calculation (see below). The very strong Raman bands at ~205 and ~335 cm$^{-1}$ (the latter giving rise to a doublet in $PNb_2S_{10}$) are assigned to $\nu$Nb–Nb and $\nu_s$Nb–$(S_2)_2$ symmetric modes, and the intense infrared bands at 318 and 329 cm$^{-1}$ in $PNb_2S_{10}$ and $P_2Nb_4S_{21}$, respectively, are attributed to the corresponding out-of-phase Nb–$(S_2)_2$ stretching $B_{2u}$ modes. The isolated absorption bands near 366 cm$^{-1}$ (resolved into a multiplet in $PNb_2S_{10}$) correspond to the $B_{1u}$ $\nu_a$Nb–$S_2$ ($M_8$) mode, and its $B_{2g}$ in-phase Raman counterpart, $M_5$ vibration, appears at slightly lower frequencies. Also, several medium- or weak-intensity bands in the range 300–240 cm$^{-1}$ can be assigned to other cluster vibrations (Table III). Finally, additional Raman bands at 311 cm$^{-1}$ in $PNb_2S_{10}$ and at 320 cm$^{-1}$ in $P_2Nb_4S_{21}$ (without infrared component) are observed for the first time. We attribute these new bands to $\nu$Nb–$S_2$ intercluster (or intrachain) symmetric vibrations, and their low frequency can be related to the slightly larger (+0.08 Å) bond lengths involved as compared with the intracluster Nb–$S_2$ distances.
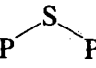
Most of the ($Nb_2(S_2)_2$) unit vibrations in the Raman spectra of $PNb_2S_{10}$ were found to be enhanced when changing the exciting laser radiation, due to preresonance effects with the intense electronic charge-transfer transition at ~405 nm (Fig. 11). Unfortunately, similar effects were not evidenced with the highly colored $P_2Nb_4S_{21}$ compound and satisfactory Raman results were only obtained using the 514.5-nm line (Fig. 10).
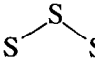
A comparison of the remaining positions (Table III) with available spectroscopic data for $(P_2S_7)^{4-}$ (*17*) and $(PS_4)^{3-}$ (*22, 23*) reveals that spectra of $PNb_2S_{10}$ and $P_2Nb_4S_{21}$ can be better understood in terms

of linked $(PS_3)$ groups rather than using a model of interacting $(PS_4)$ tetrahedra. The great multiplicity of bands in the high-frequency region, 620–400 cm$^{-1}$, affords strong support for the first model meanwhile the characteristic frequency pattern and relative intensities known for the fundamental modes in several $(PS_4)^{3-}$ salts are not encountered. The numerous high-intensity infrared bands at 600–520 cm$^{-1}$ are thus assigned to asymmetric $\nu_a PS_3$ vibrations, and the corresponding symmetric Raman intense modes are localized around 410 cm$^{-1}$ as in $Ag_4P_2S_7$ spectra. In this respect, the very strong band at 454 cm$^{-1}$ (infrared) and at 389 cm$^{-1}$ (Raman) due to $\nu$ P$\overset{\displaystyle S}{\phantom{.}}$P vibrations in $(P_2S_7)^{4-}$ anions (and previously discussed in the spectra of the $P_2NbS_8$ systems) are now missing since simple sulfur-bridged P$\overset{\displaystyle S}{\diagup\diagdown}$P bonds do not exist in $PNb_2S_{10}$ and $P_2Nb_4S_{21}$ crystal structures. Finally, some deformation modes of the $(PS_3)$ groups must contribute to the sets of bands observed in the region 300–230 cm$^{-1}$, and they overlap in part with other $(Nb_2(S_2)_2)$ cage vibrations. Some additional weak bands at ~460 cm$^{-1}$ (infrared, Raman), 424 cm$^{-1}$ (Raman), and 227 cm$^{-1}$ (Raman), only detected in $P_2Nb_4S_{21}$ spectra, are still remaining, and we propose to assign these bands to the stretching ($\nu_a$, $\nu_s$) and bending ($\delta$) vibrations of intraanionic $(S_3)^{2-}$ groups. Such a result is in agreement with spectroscopic data already known in $BaS_3$ (24), in spite of the variations of the S$\overset{\displaystyle S}{\diagup\diagdown}$S angle and bond lengths (mean values are equal to 101° and 2.028 Å, respectively, compared to 114.9° and 2.076 Å in $BaS_3$) and the fact that strong constraints in 2D $P_2Nb_4S_{21}$ are likely to exist.

Finally, it may be noted that many low-frequency Raman bands were detected in both $PNb_2S_{10}$ and $P_2Nb_4S_{21}$. Although no precise assignments can be made, these bands must originate from intrachain and interchain bending modes.

## Correlations between Vibrational and X-Ray Data and Future Outlooks

Discarding the high- and low-frequency parts of the spectra (combinations and lattice + deformation modes), we have shown in this study that the vibrational spectra are essentially a juxtaposition of bands characteristic of the niobium cluster units and of those of the anionic species. This result confirms not only the proposed descriptions of the crystal structure in terms of ionic fragments but also the predominance of nearest-neighbor interactions of covalent character.

As far as metal cage units are concerned, a close relationship between the four materials is evidenced, and the spectra are nicely interpreted using the $(Nb_2(S_2)_2)$ cluster model. The $\nu S_2^{2-}$ stretching frequencies correlate well with $d(S-S)$ bond distances, as shown in Fig. 12, and we find a good agreement with Steudel's empirical equation (25) $\nu S-S/cm^{-1} = (2.57 - d(S-S)/Å)/9.47 \times 10^{-4}$ (see the solid line in Fig. 12). Other available data on related trisulfide $MS_3$ systems ($M^{4+}$ = Nb, Ti, Zr, Hf) which also have $S_2^{2-}$ pairs within prismatic surroundings of metal ions (26–29) do not fit very well the same empirical rule. We conclude that the $\nu S-S$ modes in the systems under study appear to be characteristic and weakly coupled diatomic vibrations. Moreover, small differences on the frequency scale were observed between the in-phase $A_g$ and out-of-phase $B_{3u}$ components. As in $NbS_2Cl_2$ (8), this can be explained by weak direct interactions not only between the orbitals of both $S_2^{2-}$ pairs in a cage, but also between the different ions because of the strong covalent bonding with niobium atoms.

In spite of similar Nb–Nb bond lengths in these four compounds (2.86–2.87 Å) and in $NbS_2Cl_2$ (2.87 Å), the $\nu Nb-Nb$ vibrations are shifted either toward lower frequencies (205 cm$^{-1}$) in the 2D phases or toward higher frequencies (~222 cm$^{-1}$) in 3D $P_2NbS_8$ than its value of 214 cm$^{-1}$ in $NbS_2Cl_2$. Although these variations are
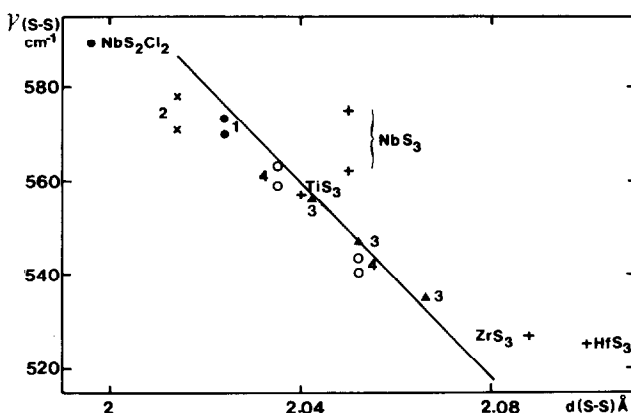
FIG. 12. Variation of the $\nu$S–S stretching vibrations versus interatomic distances, $d$(S–S), in the compounds under study [(1) 2D $P_2NbS_8$, (2) 3D $P_2NbS_8$, (3) 2D $PNb_2S_{10}$, (4) 2D $P_2Nb_4S_{21}$] and in related $NbS_2Cl_2$ and $MS_3$ systems. The solid line corresponds to Steudel's equation (see text).

quite small, we believe that the highest frequency observed in 3D $P_2NbS_8$ may come from the existence of constraints in relation to the compacity of this three-dimensional network. In this respect, it is difficult to estimate the influence of vibrational couplings and of short-range interactions, but it must be pointed out that most of the cluster-mode frequencies in 2D and 3D $P_2NbS_8$ are weakly perturbed compared to their values in the other layer structures which possess ($Nb_2S_9$) infinite chains and inter-cluster $S_2^{2-}$ pairs. We thus conclude that these cluster frequencies are weakly dependent on the different anionic surroundings. In Table IV we have collected the observed frequencies of in-phase $\nu_a$ ($M_5$–$B_{2g}$) and $\nu_s$ ($M_2$–$A_g$) Nb–$(S_2)_2$ stretching vibrations and also of the intercluster $\nu$Nb–$S_2$ modes with corresponding metal–sulfur bond lengths. In addition, the corresponding values of two $A_g$ modes which possess a dominant contribution of $M$–$S_2$ bond stretching (according to calculations of potential energy distributions) in related $MS_3$ compounds (26–29) are included. A rough frequency–distance correlation is apparent in all $Nb^{4+}$ ($d_1$)-containing compounds in which the Nb–S interactions are nearly equivalent,

while metal–sulfur force constants must be weaker in $M^{4+}$ ($d^0$)-containing trisulfur systems.

Concerning now the consequences of structural and electronic perturbations which can take place upon further interca-

TABLE IV

DEPENDENCE OF $\nu$Nb–$S_2$ VIBRATIONS (cm$^{-1}$) ON MEAN INTERNUCLEAR DISTANCES $d$ (Nb–S) (Å) IN P–Nb–S PHASES, $NbS_2Cl_2$, AND RELATED $MS_3$ SYSTEMS

| | Modes | $\nu$ (cm$^{-1}$) | $d$/Å | Ref. |
|---|---|---|---|---|
| 2D $P_2NbS_8$ | $M_2$ | 329–325 | } 2.50 | |
| | $M_5$ | 352–346 | | |
| 3D $P_2NbS_8$ | $M_2$ | 332–328 | } 2.50 | |
| | $M_5$ | 353–343 | | |
| 2D $PNb_2S_{10}$ | $M_2$ | 342–332 | } 2.495 | |
| | $M_5$ | 364 | | |
| | intercluster | 311 | 2.575 | |
| 2D $P_2Nb_4S_{21}$ | $M_2$ | 331 | } 2.495 | |
| | $M_5$ | 345 | | |
| | intercluster | 320 | 2.58 | |
| $NbS_2Cl_2$ | $M_2$ | 332–337 | } 2.485 | |
| | $M_5$ | 354 | | |
| $NbS_3$ | $A_g$ | 350 | } 2.55 | (26) |
| | $A_g$ | 340 | | |
| $TiS_3$ | $A_g$ | 300 | } 2.50 | (28) |
| | $A_g$ | 278 | | |
| $ZrS_3$ | $A_g$ | 280 | } 2.60 | (27) |
| | $A_g$ | 275 | | |
| $HfS_3$ | $A_g$ | 275 | } 2.60 | (29) |
| | $A_g$ | 261 | | |

lation reactions in these 2D phases, these vibrational results deserve some comments. If an electronic localization on P–S bands or structural distortions on $(PS_4)$ units occur upon intercalation, changes should be mainly detected in the infrared spectra where terminal $\nu PS_2$ and $\nu PS_3$ vibrations give rise to intense absorption bands. In the same way, perturbations of the bridged

$$S$$

P      P bonds in 2D $P_2NbS_8$ could be evidenced on the intense infrared and Raman signals at ~400 cm$^{-1}$. Now, if $(Nb_2(S_2)_2)$ cages play the role of electronic acceptors, great modifications must occur in both the infrared and Raman spectra in relation to observed intense cluster modes, such as the $\nu_s Nb–(S_2)_2$ $A_g$ and $B_{2u}$ components. In particular, an electronic perturbation on the $S_2^{2-}$ pairs or on the metal centers could be detected by observing the $\nu S–S$ or $\nu Nb–Nb$ vibrations. In this respect, we must mention that the UV-visible spectra should be also highly informative, since one can expect in the intercalates a modification of the lower energy $d–d$ type transitions and also of the higher energy metal-to-sulfur charge-transfer transitions, so that the guest–host lattice interactions could thus be investigated.

## Acknowledgments

## References

1. P. GRENOUILLEAU, R. BREC, M. EVAIN, AND J. ROUXEL, Rev. Chim. Miner. 20, 628 (1983).
2. M. EVAIN, R. BREC, G. OUVRARD, AND J. ROUXEL, Mater. Res. Bull. 19, 41 (1984).
3. R. BREC, P. GRENOUILLEAU, M. EVAIN, AND J. ROUXEL, Rev. Chim. Miner. 20, 295 (1983).
4. R. BREC, M. EVAIN, P. GRENOUILLEAU, AND J. ROUXEL, Rev. Chim. Miner. 20, 283 (1983).
5. Y. MATHEY, R. CLÉMENT, C. SOURISSEAU, AND G. LUCAZEAU, Inorg. Chem. 19, 2773 (1980).
6. O. POIZAT, C. SOURISSEAU, AND Y. MATHEY, J. Chem. Soc. Faraday Trans. 1 80, 3257 (1984), and references therein.
7. H. SCHÄFER AND W. BECKMANN, Z. Anorg. Allg. Chem. 347, 225 (1966).
8. J. RIJNSDORP, Ph.D. thesis. Gröningen, 1978.
9. J. RIJNSDORP, G. J. DE LANGE, AND G. A. WIEGERS, J. Solid State Chem. 30, 365 (1973).
10. C. PERRIN, A. PERRIN, AND J. PRIGENT, Bull. Soc. Chim. 8, 3086 (1972).
11. C. PERRIN, A. PERRIN, AND P. CAILLET, J. Chim. Phys. 70, 105 (1973).
12. D. W. BULLET, J. Phys. C 13, 1267 (1980).
13. I. R. BEATTIE, T. R. GILSON, AND G. A. OZIN, J. Chem. Soc. A, 2765 (1968).
14. P. GARD AND C. SOURISSEAU, unpublished results.
15. P. STEIN, V. MISHOWSKI, W. H. WOODRUFF, J. P. GRIFFIN, K. G. WERNER, B. P. GABER, AND T. G. SPIRO, J. Chem. Phys. 64, 2159 (1976).
16. R. J. H. CLARK AND C. SOURISSEAU, Nouveau J. Chim. 4, 287 (1980).
17. C. SOURISSEAU, unpublished results.
18. C. WIBBELMANN, W. BROCKNER, B. EISENMANN, AND H. SHÄFER, Z. Naturforsch. B 38, 1575 (1983).
19. R. BOCKER AND W. BROCKNER, Z. Naturforsch. A 39, 1120 (1984).
20. M. TRANQUILLE AND M. FOUASSIER, J. Chem. Soc. Faraday Trans. 2 76, 26 (1980).
21. M. SOMER, W. BUES, AND W. BROCKNER, Z. Naturforsch. A 38, 163 (1983).
22. H. BÜRGER AND H. FALIUS, Z. Anorg. Allg. Chem. 363, 24 (1968).
23. U. PATZMANN AND W. BROCKNER, Z. Naturforsch. A 38, 27 (1983).
24. G. J. JANZ, E. RODUNER, J. W. COUTTS, AND J. R. DOWNEY, Inorg. Chem. 15, 1751 (1976).
25. R. STEUDEL, Angew. Chem. Int. Ed. 14, 655 (1975).
26. A. ZWICK, M. A. RENUCCI, R. CARLES, N. SAINT-CRICQ, AND J. B. RENUCCI, Physica B 105, 361 (1981).
27. C. SOURISSEAU AND Y. MATHEY, Chem. Phys. 63, 143 (1981).
28. D. W. GALLIARDT, W. R. NIWEEN, AND R. D. KIRBY, Solid State Commun. 34, 37 (1980).
29. S. P. GWET, Y. MATHEY, AND C. SOURISSEAU, Phys. Status Solidi B 123, 503 (1984).